Assessment of Multi-Axial Stress State effects of Circular Concrete-Filled Steel Tubular Columns under Flexural Loading

Yadong Jiang António Silva Bledar Kalemia
José Miguel Castro Ricardo Monteiro

Abstract

The paper proposes the methodologies and the equations to consider the influence of multi-axial stress states on the material strength of circular Concrete-filled Steel Tubular (CFST) columns. The combination of multi-axial stress states, namely the concrete confinement effects and the steel bi-axial stress state, is found to benefit the bending capacity of circular CFST columns. Therefore, to account for the material strength variation under multi-axial stress states and to improve the accuracy of the previous proposed Distributed Plasticity (DP) model, material strength correction methods are proposed based on the analytical results given by the 3D Finite Element (FE) model. A comprehensive parametric study, which involved a wide range of diameter-thickness ratios, material properties and axial load levels, has been carried out to study the influence of CFST cross-section properties on the multi-axial stress states. Based on the parametric study, the confined concrete strength under bending is found to be independent of the constant axial load level. On the contrary, the steel bi-axial stress is proved to be sensitive to the cross-section axial load. A section factor ξ is used to represent both the geometry and material properties of a CFST cross-section. With statistic operations, ξ-dependent correction equations are derived to account for the material strength variation under multi-axial stress states. The feasibility of the proposed material strength correction equations is verified to be good for both the design and modelling of circular CFST members.

1 Introduction

The behaviour of concrete-filled steel tubes (CFSTs) is governed by the contribution of the steel tube and the concrete core. As concluded from previous experimental studies (Silva et al. 2016 [1] and Silva et al. 2017 [2]), The concrete core constrains the steel tube to its interior, thus delaying the occurrence of the local buckling to higher levels of deformation and the ductility of the steel tube is improved. Besides its excellent ductility, the composition of concrete and steel will also cause the two components under multi-axial stress state and thus, lead to the material properties variance. The steel tube provides the confining stress to the concrete core and makes it under tri-axial stress state, which is well known as concrete confinement effect. The strength and ductility of the concrete core are enhanced by the

confinement effect, therefore, the capacity of CFST member under either compression or bending is benefited. In recent years, there were many researchers had investigated the concrete confinement effect of CFST members. Based on the test results, Sakino et al. 2004 [3], Fujimoto et al. 2004 [4] and Inai et al. 2004 [5] had tested circular and rectangular CFST columns under axial compressive loading, eccentric compressive loading and bending, respectively. All the researchers figured out that, the circular CFST members had a more significant concrete confinement effect than the rectangular columns. Hu et al. 2003 [6] and Hu et al. 2005 [7] had derived the equations to calculate the confined concrete strength under either compression or bending. The concrete confinement effect of CFST member was found to be sensitive to its diameter-thickness ratio. Regarding Eurocode 4 [8], the concrete confinement effect of circular CFST members is considered in both compressive and bending cases.

Due to the expansion of the concrete core, the steel tube of CFST will be under bi-axial stress state when the member is loaded. The bi-axial stress state will have an influence on the steel yield stress. According to the research works of Fujimoto et al. 2004 [4] and Inai et al. 2004 [5], the bi-axial stress state would increase the steel yield stress when the CFST member is under tension while decrease the steel yield stress when the member is compressed. Regarding the Eurocode 4 [8] design provision, it considers a reduction of the steel yield stress when calculating the circular CFST column's plastic resistance to compression. While for the consideration of the flexural resistance of the circular CFST member, the Eurocode 4 is very restrictive since the code does not consider any effects of steel bi-axial stress state to exist.

The Distributed Plasticity (DP) model is a widely used modelling choice for CFST columns. As the DP model is a simplified numerical solution coupled with fibre element, it could not capture the multi-axial stress states, for both concrete core and steel tube. Therefore, the material properties of CFST should be corrected when applying the DP model. In recent studies of CFST columns, all the researchers (Han 2004 [9], Fujimoto et al. 2004 [4], Inai et al. 2004 [5], Liang et al. 2006 [10], Valipour and Foster 2010 [11], Tort and Hajjar 2010 [12], Zubydan and ElSabbagh 2011 [13], Lai and Varma 2016 [14], etc.) who worked with DP model had considered the concrete strength under confinement effect. But regarding the steel bi-axial stress, only Fujimoto et al. 2004 [4], Inai et al. 2004 [5] and Lai and Varma 2016 [14] had considered its influence on the steel yield stress during modelling. The neglecting of steel bi-axial stress states of CFST member may miss leading the analytical results and decrease the accuracy of the DP model.

As one may have inferred, there is a clear gap in the consideration of multi-axial stress states, including both concrete confinement effect and steel bi-axial stress state, when model or design the CFST members under flexural loads. The research presented in this paper aims to address this limitation of both the literature and the current design methodologies. This paper starts with a brief description of the multi-axial stress states and the verification of the previously proposed material strength correction method for CFSTs. Based on the 3D Finite Element (FE) model proposed in Jiang et al. 2018 [?], New material strength correction methods, which aims to overcome the aforementioned limitations of the DP model, are developed and validated. By conducting a parametric study on the flexural behaviour of circular CFST members, closed-form expressions which focus on the calculation of the confined concrete stress and the steel bi-axial steel bi-axial yield stress are derived and their

feasibility is verified against experimental data.

2 Multi-axial Stress States of Circular CFST Members

2.1 Multi-axial Stress States

When the CFST members are under loading, the composite effects are introduced due to the interaction between concrete core and steel tube. Thus, both the concrete and steel are under the multi-axial stress states. The confined stress provided by the steel tube makes the concrete core under tri-axial stress state, and thus, caused the concrete confinement effect, which can improve its the strength and ductility. Thus, the concrete confinement effect will benefit the flexural capacity of CFST members. There were many researchers studied the concrete confinement effect for CFST members in recent years (Han et al. 2001 [15], Hu et al. 2003 [6], Hu et al. 2005 [7], Tort and Hajjar 2010 [12] and Lai and Varma 2016 [14]).

Not only the concrete core but also the steel tube is under multi-axial stress state. The concrete core expands under axial load and the hoop stress (or circumferential stress) is generated around the steel tube. As the thickness of the steel tube is relatively small compared to the cross-section diameter, the steel tube could be considered as a shell component. Therefore, the material is under bi-axial stress state (Kwan et al. 2016 [16]). Figure 1 shows the stress state of the steel tube of circular CFST member. Since the CFST member is under bending, part of the steel tube is under compression and part of it is under tension and the influences of bi-axial stress state on the two parts are different. As can be seen in Figure 1, for the compression area, the steel is combined with the compressive stress on the vertical direction (σ_2) and tensile stress on the horizontal direction (σ_1). While for the tension area, the steel is under tensile stress on both vertical and horizontal directions.

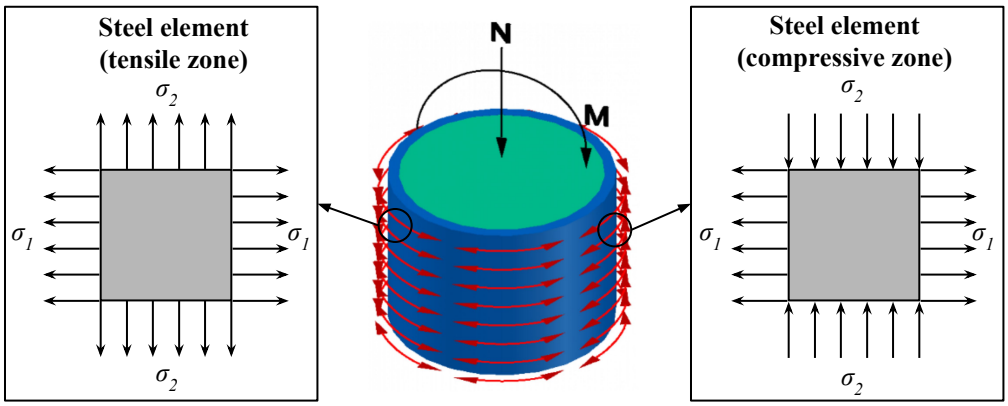

Figure 1: Steel bi-axial stress state under bending force

To consider the steel yield stress variance under bi-axial stress state, the yield surface is introduced (Figure 2). The positive/negative values on the two axes stand for the tensile/compressive stress, respectively. The hoop stress (σ_h) is plotted on the x axis and the corresponding steel yield stresses under compression (f_{yc}) and tension (f_{yt}) are annotated on the yield surface. It could be found that the steel compressive yield stress (f_{yc}) is smaller

than the uniaxial yield stress (f_y), which will have a negative influence on the member flexural capacity. On the contrary, the steel tensile yield stress (f_{yt}) is larger than the uniaxial yield stress (f_y), which will benefit the member strength under bending. For circular CFST member under central compression, the whole steel section is under compression. With the influence of bi-axial stress state, the steel yield stress reduces from f_y to f_{yc}. For this reason, there is a reduction factor introduced in Eurocode 4 [8] to reduce the steel yield stress when considering the plastic resistance of circular CFST to compression. Regarding the flexural capacity of CFST members, the influence of the steel bi-axial stress state on it depends on the relative areas between the compressive/tensile regions as well as the values of f_{yt} and f_{yc}.

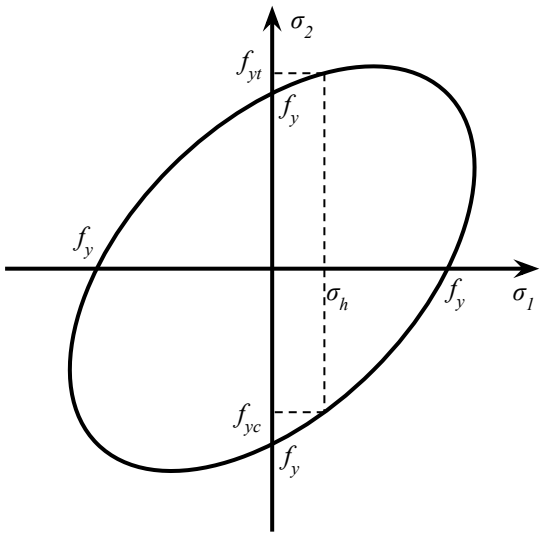

Figure 2: Steel yield surface

The previous research (Jiang et al. 2018 [?]) had carried out a numerical study on the influence of the multi-axial stress states on the bending capacity of circular CFST columns. In the research work, a comprehensive 3D Finite Element (FE) model, which can capture the multi-axial stress states, and a Distributed Plasticity (DP) model, which cannot consider the multi-axial stress states influence, were developed and validated by experimental results from Silva et al. 2016 [1]. The 3D FE model was proved to be accurate on the flexural behaviour simulation of the circular CFST member, as the solid and shell elements used by the model can consider the concrete and steel strength variation under multi-axial stress states. But regarding the DP model, its predicted capacity was found to be always smaller than the test results. Considering that the effects caused by multi-axial stress states could not be simulated by the fibre element, the researchers concluded that the combination of multi-axial stress states could benefit the bending behaviour of circular CFST member under bending combined with low/moderate constant axial load.

To further verify the influence of the steel bi-axial stress state on material strength, the stress versus strain curves of the steel elements located on the same height level are extracted and plotted in Figure 3. The steel uniaxial stress/strain curve is also plotted in the same figure as the reference curve. The tensile strain/stress are defined as positive values. It

could be seen that the steel compressive yield stress values are less than the uniaxial yield stress and the tensile yield strain is larger than the uniaxial yield stress, which enhances the conclusion obtained from the yield surface.

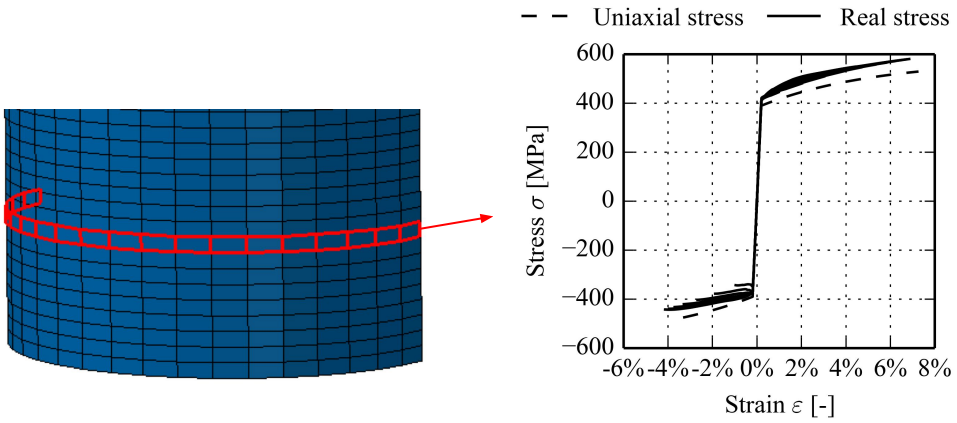

Figure 3: The vertical stress/strain curves output from the 3D FE model

2.2 Previous Studies on Multi-axial Stress State Influence

In the past, there were many researchers had carried out the studies on the prediction of confined concrete strength for CFST members (Han et al. 2001 [15], Hu et al. 2003 [6], Hu et al. 2005 [7] and Tort and Hajjar 2010 [12] e.t.c). But in these research works, the influence of steel bi-axial stress state was ignored. Therefore, these derived confined concrete strength equations may result in the inaccuracy of the numerical prediction. Lai and Varma 2016 [14] had performed a parametric study on CFST members under compressive loading with the consideration of multi-axial stress states. The equation to calculate the confined concrete strength had been derived. Moreover, the steel compressive yield strength in the research was reduced to $0.9f_y$. But regarding the steel tensile yield stress, there was no correction. Thus, the proposed material strength correction equations of Lai and Varma 2016 [14] were suitable for CFST members subjected to axial compression but not sufficient for members under bending.

Inai et al. 2004 [5] and Fujimoto et al. 2004 [4] had used the DP model to simulate the bending behaviour of CFST members. To consider the influences of multi-axial stress states, they combined the previous researches on the confined concrete strength and the steel bi-axial yield stress (Kato and Nishiyama 1980 [17], Sakino 1994 [18], Nakahara et al. 1999 [19] and Sakino et al. 1998 [20]) and summarized the material strength correction equations for both concrete and steel. For circular CFST members, the confined concrete strength is given in Equation (1).

$$f_{cc} = f_c + 4.1\frac{0.38tf_y}{D-2t} \tag{1}$$

Regarding the steel bi-axial stress state, a constant hoop stress, which equals to $0.19f_y$, was assumed and the steel yield stresses under compression and tension were adopted as

$0.91f_y$ and $1.08f_y$, respectively. The proposed DP models from Jiang et al. 2018[?] were re-analysed with the material strengths corrected by these equations to verify their accuracy. Table 1 shows the confined concrete strength (f_{cc}) and the corrected steel yield stresses (f_{yc} and f_{yt}).

Table 1: Corrected material strength for the circular CFST specimens with methololedges from Inai et al. 2004 [5] and Fujimoto et al. 2004 [4]

Figure 4 displays the lateral load versus drift ratio plots comparison of three results, namely the tests results, the DP model results with uniaxial material strength and the DP model results with corrected material strength. The four plots on the left column of the figure belong show the response of the CFST specimens with no axial load. It could be found that, with the correction methods given by Inai et al. 2004 [5] and Fujimoto et al. 2004 [4], the accuracy of the DP model had been improved, as good agreements are observed between the DP model with corrected material strength and the test results. But regarding the specimens with constant axial loads (plots on the right column), nearly no improvement of the DP model results is found by applying the correction methods, by comparing its results with the original DP model predictions. As constant factors were used to correct the steel stress in the correction methods given by the two research works, it could be summarized that the steel bi-axial stress state has a relationship with the axial load level.

3 Material Strength Correction Methods

As concluded in Section 2, the material strength correction methods proposed by previous researchers are not efficient enough to improve the prediction results of the DP model, especially in the cases that the circular CFST members are loaded with lateral force combined with a constant axial load. Thus, new material strength correction methods should be proposed to account for the influence of the multi-axial stress states on the material strength variance of the circular CFST member. Given that the developed 3D FE model (Jiang et al. 2018 [?]) can accurately represent the flexural behaviour of CFST members, this model is used to calibrate this strength correction methodology. In the following paragraphs, the material strength correction methods, which aims to acquire the confined concrete strength (f_{cc}) and the steel bi-axial yield stress (f_{yb}) from the numerical results given by the 3D FE model, are detailed.

3.1 Overall Description of the Approach

The material strength correction methods are applied to the base section of the CFST column. As the multi-axial stress states have different influences on the concrete and steel properties, the two sections should be analysed in a separate manner. For each of the two sections, two steps are followed to get the corrected material strength, namely to address the yield moment of the section and to adopt the equivalent (or average) stress of the section at the yield point. Figure 5 shows the schematic diagram of the strength correction methods. Taking the advantages of the 3D FE model, the moment-drift and axial force-drift curves

of both the concrete section and steel tube section can be extracted from the numerical results, where the drift ratio (θ) is defined as the ratio between the lateral displacement and the CFST column length (L). It should be noted that, although the individual axial loads applied to the concrete and steel sections change with the increase of the drift ratio, the sum of the axial loads on the two sections is equal to a constant axial load applied to the CFST member. Due to the algorithm behind the 3D FE analysis, the outputs of the results are sets of discrete incremental values. Thus, the method proposed by Akima 1970 [21] is introduced to smooth these force-drift curves by interpolation. For the two cross-sections, their yield drift ratios ($_y^c$ and $_y^s$) of the moment-drift plots could be adopted. The corresponding section moments (M_y^c and M_y^s) and axial loads (N_y^c and N_y^s) could be acquired. By making reasonable assumptions about the stress distributions on the concrete and steel sections, which are described in Sections 3.3, the equivalent stresses of the two sections at the yield points could be calculated based on the section force equilibrium. The two adopted equivalent stresses are taken as the corrected material strengths. In the following sections, the correction methods for each of the member parts are detailed.

3.2 Yield Points of the Concrete and Steel Sections

The yield moments of the concrete core and the steel tube are directly related to their material strengths, namely the confined concrete strength and the steel bi-axial yield stress. Thus, to acquire the corrected material strengths, the yield points of the two sections should be addressed first. Figure 6 shows the moment-drift ratio curves of the concrete section. The shape of the moment-drift ratio curve can be classified into two types. For the concrete core with a relatively high confining stress, not only its strength but also its ductility is remarkably increased. Thus, the corresponding moment-drift ratio curve shows no strength degradation at the plastic range, as can be seen in Figure 6 (a). While for the concrete core under low/moderate confinement effect, although its strength and ductility are improved by the confined stress, the confined stress level is not enough to eliminate the influence of the concrete cracks. Thus, there is still strength degradation exhibited in the corresponding moment-drift ratio curve (Figure 6 (b)). For the two conditions, the correction methods are slightly different.

The method to find the yield point of the concrete section is proposed by ECCS 1986 [22], which used the tangent value to adopt the yield force and displacement of the curve. As marked in Figure 6 (a) and (b), the point ($_y^c$, M_y^c), which has the tangent value equalling to 10% of the initial slope of the curve, is adopted as the yield point of the concrete section. Regarding the initial slope, its value equals to the slope of the line which connects the point with $0.4M_{max}^c$ strength to the coordinate origin. For the concrete core with the moment-drift ratio curve type shown in Figure 6 (a), the axial load N_y^c corresponding to drift ratio $_y^c$ could be adopted and the axial load and moment pair (N_y^c, M_y^c) is taken as the section force to acquire the confined concrete strength f_{cc}, which is detailed in Section 3.3. Regarding the concrete core with the moment-drift ratio curve type similar to the Figure 6 (b), the influence of the section strength degradation should be considered. The yield moment M_y^c should be compared with the residual moment M_{res}^c. If the residual moment M_{res}^c is smaller than the yield moment M_y^c, the axial load and moment pair (N_{res}^c, M_{res}^c) should be taken as the section forces to adopt the confined concrete strength instead of using force pair (N_y^c, M_y^c).

By taking into account the influence of the residual moment M^c_{res}, the acquired confined concrete strength should stay on the safe side.

Figure 7 shows the moment-drift ratio curve of the steel cross-section. As can be seen, the method of adopting the yield point of the steel cross-section is similar to the method applied to the concrete core, which makes use of the tangent value. The moment-drift ratio curve of the steel cross-section shows good ductility due to the constraint effects of the concrete core. The influence of residual strength can be neglected and the force pair (N^s_y, M^s_y) is used to adopt the steel bi-axial stress, which is described in the following section.

3.3 Corrected Material Strength

With the yield points adopted from Section 3.3, the corrected material strengths of the concrete and the steel can be obtained by conducting section analysis. As observed in Jiang et al. 2018 [?], for CFSTs under flexural loading, the stress distributions on the cross-sections are non-uniform. Due to this non-uniformity, it may be difficult to pinpoint the location of the neutral axis of the cross-section. Thus, although the stress distribution on the two sections could be extracted from the numerical results easily, it is not recommended to adopt the corrected material strengths from the non-uniform distributed stress. Therefore, to perform any material strength correction, the non-uniform stress distribution should be converted into a uniform distribution of stresses for both sections. Figure 8 shows the simplified stress blocks of the concrete and steel tube sections according to the assumptions made in Section 3.3.1 and 3.3.2. The uniform distributed stress values on the concrete and the steel cross-sections, which represent the average stress on the two sections, are adopted as the corrected material strengths of the CFST member. In the following subchapters, an indirect approach is proposed to obtain the corrected material strengths of the concrete and steel sections.

3.3.1 Corrected Material Strength of Concrete

Regarding the concrete core, the following assumptions are made:

- The cross-section has reached a full plasticity state;
- The tensile strength of the concrete is neglected, since it is relatively low compared to the compressive strength, and in the likely event of cracking, no stresses will develop in the tensile region;
- The confined concrete stresses are uniformly distributed in the compressive region with a value of f_{cc}, which is the equivalent stress shown in Figure 8;
- The neutral axis is a straight line parallel to the bending axis, i.e. perpendicular to the lateral loading direction. The distance from the neutral axis to the major axis of the section is h_c, which ranges from $0.5D_c$ to $0.5D_c$, as shown in Figure 8.

Based on the equilibrium of axial loads and moments shown in Equation (2) and supplementary Equations (3) to (5), the confined concrete strength, f_{cc}, could be calculated.

$$\begin{cases} N^c_y + A_{cc} f_{cc} & = 0 \\ M^c_y + A_{cc} f_{cc} h_{cc} & = 0 \end{cases} \text{or} \begin{cases} N^c_{res} + A_{cc} f_{cc} & = 0 \\ M^c_{res} + A_{cc} f_{cc} h_{cc} & = 0 \end{cases} \tag{2}$$

Table 2: Corrected material strengths from the correction methods

$$A_{cc} = \frac{1}{4}\theta_c D_c^2 + \frac{1}{2}h_c D_c \sin\theta_c \tag{3}$$

$$h_{cc} = \frac{2(\frac{D_c^2}{4} - h_c^2)^{\frac{3}{2}}}{3A_{cc}} \tag{4}$$

$$\theta_c = \cos^{-1}\frac{2h_c}{D_c} \tag{5}$$

3.3.2 Corrected Material Strength of Steel

As concluded in Section 2.1, the steel bi-axial stress state will make the steel has different yield stresses under compression and tensile force. But in modelling or design of CFST members, it is no common to consider the steel compressive and tensile yield stresses individually. Thus, the average stress of the steel section at yield point, which is the uniform distributed stress value in 8, is adopted to represent the steel bi-axial stress (f_{yb}). To perform the strength correction method, the following assumptions about the stress distribution on the steel section are made:

- The whole cross-section is in plasticity state;
- Compressive and tensile stresses are assumed to have the same absolute value, f_{yb}, which is the steel bi-axial yield stress;
- The neutral axis is a straight-line parallel to the bending axis. The distance from the neutral axis to the major axis of the section is hs, which ranges from $0.5D$ to $0.5D$, as shown in Figure 8.

Based on the equilibrium of axial loads and moments shown in Equation (6) and the corresponding supplementary Equations (7) to (16), the steel bi-axial yield stress, f_{yb}, could be calculated as:

3.4 Validation of the Correction Methods

In order to validate the proposed material strength correction methods for circular CFST members, the eight specimens used in Section 2.2 were applied with the methods. The original and the corrected material strengths are listed in Table 2. It could be found that both the concrete and the steel yield strengths are increased by the proposed correction methods, which is in line with the conclusion that the multi-axial stress states will have a positive influence on the flexural capacity of the circular CFST member.

The eight specimens are re-analysed by the DP model with the material strengths given by the correction methods. As discussed in Section 3.2, the correction methods have already taken the influence of concrete residual strength into consideration during correction procedure. Thus, the acquired confined concrete strength stays on the safe side and there is no

Table 3: Effect of strength corrections on DP modelling peak flexural capacities

need to consider the softening of the concrete strength for the second time. Therefore, the confined concrete constitution law used in DP model is defined as a perfect elasto-plastic curve. The obtained lateral force-drift curves of the eight specimens are shown in Figure 9. For each member, the numerical results of the DP model with both the uncorrected and corrected material properties (labelled with FE_{DP} and FE_{DP}^{Method}, respectively) are plotted against the results of the 3D FE model (labelled with FE_{3D}).

Analysis of the results shown in Figure 9 allows concluding that the computation of material strength corrections in the DP model leads to a very good agreement the results from the 3D FE model. This is further supported by comparing the peak lateral loads, as shown in Table 3. In the table, the maximum lateral forces of the DP models (F_{DP} for the uniaxial material strengths and F_{DP}^{Method} for the corrected material strengths), are compared with the value from the 3D FE model, F_{3D}. The ratios between the ultimate values of the 3D FE model and the DP models, F_{DP}/F_{3D} and F_{DP}^{Method}/F_{3D}, are also shown. As one may infer from the analysis of Table 3, by correcting the material strength, the average differences between the 3D FE model and the DP model decrease from 12% to 3%. Thus, it can be concluded that the strength correction method could greatly enhance the accuracy of the DP modelling approach.

4 Material Strength Correction Equations

Although the correction of material strength could improve the accuracy of the DP model, the drawback is obvious: one should conduct a detailed numerical analysis (e.g. 3D FE model) before any other analysis. Although in principle, this works for any CFST, the process itself lacks efficiency when extrapolated to a large number of members. Thus, the development of a material strength correction database, in the form of member property-dependent equations, is particularly relevant, since detailed modelling procedures need not be carried out again. In the following sections, a comprehensive parametric study aims at the development of such material strength correction database, is described. The statistic procedure is taken and the material strength correction equations, which is independent on the 3D FE model, are derived.

4.1 Parametric Study

To carry out the parametric study, a number of parameters that define both the properties of the CFST member and the load conditions were considered: 1) diameter-to-thickness ratio of the steel tube; 2) concrete uniaxial compressive strength; 3) steel uniaxial yield stress and 4) axial load level. As shown in Table 4, eleven steel tubes were adopted, between high and moderate values of diameter-to-thickness ratio. The length of the tube is fixed to six times its diameter. Four different steel grades, namely S235, S355, S420 and S690, are adopted and combined with the eleven steel tubes types. For each steel grade, two different concrete strengths were considered, namely $0.1f_y$ and $0.2f_y$, and the value is limited to a maximum

Table 4: Steel tubes of the parametric study

of $100MPa$. As a combination of the previous material parameters with the considered steel tubes, a total of 88 CFST members were adopted for the parametric study.

The axial load level will play an important role in the corrected material strength, as the increase of the axial load will result in the change of location of the neutral axis. Thus, five different axial load levels, $_n$, are adopted, namely 0% (no axial load), 5%, 10%, 20% and 30%. The axial load level is defined as the portion of the plastic axial strength of the cross-section, calculated with Equation (17).

By combining the 88 CFST columns with the 5 axial load levels, 440 monotonic flexural analysis was conducted. Each of the columns was laterally loaded up to a drift ratio level of 7%. For all the columns, the material strength correction methods described in Section 3 were applied. Thus, a material strength database consisting of 440 CFST members was created.

In order to represent the wide set of members with a single representative parameter, a section factor, , is adopted, as shown in Equation (18). In a simplified manner, the section factor consists the cross-section slenderness, D/t, unconfined concrete strength, f_c, and uniaxial steel yield stress f_y. For CFST members with given concrete and steel types, the larger values of indicate a stronger concrete core and a weaker steel tube, and vice versa.

4.2 Strength Correction Equations for Concrete

Regarding the strength corrections of the concrete core, the ratio between the confined and plain strength values, f_{cc}/f_c, are plotted against section factor in Figure 10. The scatters of the CFST members are grouped according to the axial load levels, $_n$, and are classified in different colours. Analysis of the results allows concluding that regardless of the axial load level, the values of f_{cc}/f_c were consistently larger than 1.0. This confirms the development of confinement in the concrete core, which increases the strength of the concrete material. Also clear is that as increases, f_{cc}/f_c decreases. This is in line with the common notion that the higher the cross-section slenderness (which is proportional), the least significant will the confinement effect of the concrete core be.

It could also be found that the scatter distributions of different axial load levels tended to be similar. This indicates that the confinement effect of the concrete core does not depend on the axial load level, for flexural loading scenarios. From the Figure 10, it may also be assumed that the relationship between f_{cc}/f_c and is linear. Thus, for the condition that the column is under flexural force, the confined concrete strength function of circular CFST member is proposed as Equation (19). It should be noted that, in Figure 10, there are 84% of the scatted points staying above the proposed equation line, which indicates that the confined concrete strength function can reduce the possibility of overestimating the confined concrete strength. It should be highlighted that, as concluded by Hu et al. 2003 [6] and Hu et al. 2005 [7], for CFST members under centrally compression and flexural force, the confined strength of the concrete core should be different. Thus, the proposed confined concrete strength equation only applies to the case that the circular CFST column is under bending combined with a constant axial load.

Table 5: The coefficients a_s, b_s and c_s values for each axial load level

Table 6: Corrected material strengths from the correction equations

4.3 Strength Correction Equations for Steel

Similar to the corrections of the concrete, the ratio between the steel bi-axial yield stress and uniaxial yield stress, f_{yb}/f_y, are plotted against in Figure 11 for each $_n$. Analysis of the results shown in f_{yb}/f_y allows concluding that similarly to the values for concrete, regardless of the axial load level, the values of fyb/fy were always larger than 1.0. This indicates the development of bi-axial stress state for circular CFST members under moderate/low axial load level, which benefits the member flexural capacity. Also clear is that the axial load has a negative influence on the stress state effect, as the steel bi-axial yield stress decreases with the increase of $_n$. This enhances the conclusion from Section 2.2 that the axial load level will affect the steel bi-axial stress state.

It can be observed that all the five sets of scatters have a linear trend. Thus, the least-square linear regressions are applied to the scatters of five axial load levels. The corresponding regression line coefficients a_s and b_s of the five sets of data are listed in Table 5. Based on the regression lines, the material strength equation for the steel is proposed. As expressed in Equation (20), the equation is generated by shifting the regression line downward by a value of c_s. The c_s values, which will make about 84% of the scatters above the strength equation line of each axial load level, are listed in Table 5. The main purpose of introducing the parameter c_s is to reduce the possibility of overestimating the steel bi-axial stress and thus, make the material correction equation stay on the safe side.

For one CFST column of a given axial load level, the coefficients a_s, b_s and c_s values can be adopted by conducting linear interpolation of axial load level $_n$ in Table 5. It should be highlighted that the equation only applies for circular CFST member with axial load level less than or equal to 30%.

4.4 Validation of Strength Correction Equations

In order to validate the Equations (19), (20), the DP models in Section 2.2 were remodelled using the strength given by the proposed equations. The corrected material strengths are calculated from the expressions and are listed in Table 6.

The obtained lateral force-drift ratio curves of the eight specimens are shown in Figure 12. For each member, the numerical results of the DP model with both the uniaxial and corrected material properties (labelled with FE_{DP} and FE_{DP}^{Eq}, respectively) are plotted against the results of the experimental tests. Analysis of the results shown in Figure 12 allows concluding that the computation of DP model (with the use of the material strength correction equations) leads to a good agreement against the experimental results. In general, there is an increase of the bending capacity of the CFST member when the material strength correction is considered, compared with the DP model with the uniaxial properties. In terms of accuracy, the DP model with corrected strength fits better with the experimental data, especially in the post-yield stage.

Table 7: Comparison of peak flexural capacities between the DP models and the experimental evidence

Table 8: Comparison of flexural capacities between Eurocode 4 (with and without strength correction) and experimental evidence

The benefits of applying the material strength correction equations are further supported by comparing the peak test and numerical lateral loads, as shown in Table 7. In the table, the maximum lateral forces of the DP models, F_{DP} for the uncorrected material strengths and F_{DP}^{Eq} for the corrected material strengths with the use of regression equations, are compared with the values from experimental tests, F_{test}. The ratio between the values of the test and the DP models, F_{DP}/F_{test} and F_{DP}^{Eq}/F_{test}, are also shown.As one may infer from Table 7, by correcting the material strength with the proposed strength correction equations, the average differences between the test results and the DP model decrease from 11% to 1%.

Also important is to compare how the peak bending moment measured in the tests, M_{test}, compares with the value from the Eurocode 4 with and without material strength corrections (M_{EC4} and M_{EC4}^{Eq}, respectively). The results obtained are shown in Table 8. Analysis of the results shown in Table 8 allows concluding that by computing the corrected material strengths into the design methodology of Eurocode 4, the average differences between the code and the experimental evidence reduce from 24% to 15%. The design values of all specimens are still lower than the test results, which indicates that this methodology is still on the conservative side. By comparing the experimental results, with the DP model and the design approach of Eurocode 4, both with the corrected material strengths, the significance and validity of the proposed material strength correction equations is clear.

5 Conclusions

This research paper has detailed the methodologies and the equations proposed for flexural loaded circular CFST columns, which aim to consider the material strength variance under multi-axial stress states. The influence of the multi-axial stress states, namely the concrete confinement effect and the steel bi-axial stress state, on the bending capacity of circular CFST member had been discussed. Material strength correction methods, which can acquire the confined concrete strength and steel bi-axial stress from the 3D FE model prediction, were devised and calibrated. A parametric study, which consisted of 440 CFST members under flexural loading, combined with different levels of axial load, were carried out. Given the results of the parametric study, and $_n$ dependent material strength correction equations were derived to account for the development of multi-axial stress states on both parts of circular CFST members under flexural force. Within the scope of the results obtained, the following conclusions can be withdrawn:

- Not only the concrete confinement effect but also the steel bi-axial stress state are discovered to have a positive influence on the bending capacity of circular CFST members. By validating against the experimental results, the previously developed strength

correction methods are proved to be inaccurate to consider the influence of the axial load on the multi-axial stress states;

- By validating against the results of the 3D FE model, the proposed material strength correction methods are verified to improve the accuracy of the DP model on the flexural behaviour prediction of circular CFST members;
- Based on the parametric study, it is observed that the confined concrete strength can be considered to be independent of the axial load level, for cases that the circular CFST members are under flexural forces and the constant axial load level is less than 30%;
- The development of confinement on the concrete core decreases as the proposed section factor, , increases;
- For the steel tube, it is found that the development of a bi-axial stress state on the steel tube walls may increase the uniaxial strength of the material when the axial load level $_n$ is less than 30%. The increase in axial load level is found to have a detrimental effect on the influence the bi-axial stress state;
- The proposed material correction equations are validated against experimental evidence and found to improve the accuracy of both simplified modelling and Eurocode 4 design procedures.

References

[1] A. Silva, Y. Jiang, J.M. Castro, N. Silvestre, and R. Monteiro. Experimental assessment of the flexural behaviour of circular rubberized concrete-filled steel tubes. *Journal of Constructional Steel Research*, 122(Supplement C):557 – 570, 2016.

[2] A. Silva, Y. Jiang, J. M. Castro, N. Silvestre, and R. Monteiro. Monotonic and cyclic flexural behaviour of square/rectangular rubberized concrete-filled steel tubes. *Journal of Constructional Steel Research*, 139:385–396, 2017.

[3] Kenji Sakino, Hiroyuki Nakahara, Shosuke Morino, and Isao Nishiyama. Behavior of centrally loaded concrete-filled steel-tube short columns. *Journal of Structural Engineering*, 130(2):180–188, 2004.

[4] Toshiaki Fujimoto, Akiyoshi Mukai, Isao Nishiyama, and Kenji Sakino. Behavior of eccentrically loaded concrete-filled steel tubular columns. *Journal of Structural Engineering*, 130(2):203–212, 2004.

[5] Eiichi Inai, Akiyoshi Mukai, Makoto Kai, Hiroyoshi Tokinoya, Toshiyuki Fukumoto, and Koji Mori. Behavior of concrete-filled steel tube beam columns. *Journal of Structural Engineering*, 130(2):189–202, 2004.

[6] Hsuan-Teh Hu, Chiung-Shiann Huang, Ming-Hsien Wu, and Yih-Min Wu. Nonlinear analysis of axially loaded concrete-filled tube columns with confinement effect. *Journal of Structural Engineering*, 129(10):1322–1329, 2003.

[7] Hsuan-Teh Hu, Chiung-Shiann Huang, and Zhi-Liang Chen. Finite element analysis of cft columns subjected to an axial compressive force and bending moment in combination. *Journal of Constructional Steel Research*, 61(12):1692–1712, 2005.

[8] CEN EN. *Eurocode 4: Design of composite steel and concrete structures - Part 1-1:General rules and rules for buildings*. European Committee for Standardization, 2004.

[9] Lin-Hai Han. Flexural behaviour of concrete-filled steel tubes. *Journal of Constructional Steel Research*, 60(2):313–337, 2004.

[10] Qing Quan Liang, Brian Uy, and JY Richard Liew. Nonlinear analysis of concrete-filled thin-walled steel box columns with local buckling effects. *Journal of Constructional Steel Research*, 62(6):581–591, 2006.

[11] Hamid R Valipour and Stephen J Foster. Nonlinear static and cyclic analysis of concrete-filled steel columns. *Journal of Constructional Steel Research*, 66(6):793–802, 2010.

[12] Cenk Tort and Jerome F Hajjar. Mixed finite-element modeling of rectangular concrete-filled steel tube members and frames under static and dynamic loads. *Journal of structural engineering*, 136(6):654–664, 2010.

[13] Ahmed H Zubydan and Ashraf I ElSabbagh. Monotonic and cyclic behavior of concrete-filled steel-tube beam-columns considering local buckling effect. *Thin-Walled Structures*, 49(4):465–481, 2011.

[14] Zhichao Lai and Amit H Varma. Effective stress-strain relationships for analysis of non-compact and slender filled composite (cft) members. *Engineering Structures*, 124:457–472, 2016.

[15] Lin-Hai Han, Xiao-Ling Zhao, and Zhong Tao. Tests and mechanics model for concrete-filled shs stub columns, columns and beam-columns. *Steel and Composite Structures*, 1(1):51–74, 2001.

[16] AKH Kwan, CX Dong, and JCM Ho. Axial and lateral stressstrain model for concrete-filled steel tubes. *Journal of Constructional Steel Research*, 122:421–433, 2016.

[17] B Kato and I Nishiyama. Local buckling strength and deformation capacity of cold-formed steel rectangular hollow section. *Trans. AIJ*, (294):45–51, 1980.

[18] Kenji Sakino. Stress-strain curve of concrete confined by rectilinear hoops. *Journal of structural and construction engineering, AIJ*, 461:95–104, 1994.

[19] Hiroyuki Nakahara, Kenji Sakino, and Eiichi Inai. Analytical model for compressive behavior of concrete filled square steel tubular columns. *Transactions of the Japan Concrete Institute*, 20:171–178, 1999.

[20] K Sakino, T Ninakawa, H Nakahara, and S Morino. Experimental studies and design recommendations on concrete filled steel tubular columns: Us-japan cooperative earthquake research program. In *Structural Engineers World Congress*. Amsterdam ; New York : Elsevier, 1998.

[21] Hiroshi Akima. A new method of interpolation and smooth curve fitting based on local procedures. *J. ACM*, 17(4):589–602, October 1970.

[22] ECCS. *Recommended testing procedure for assessing the behviour of structural steel elements under cyclic loads*. 1986.

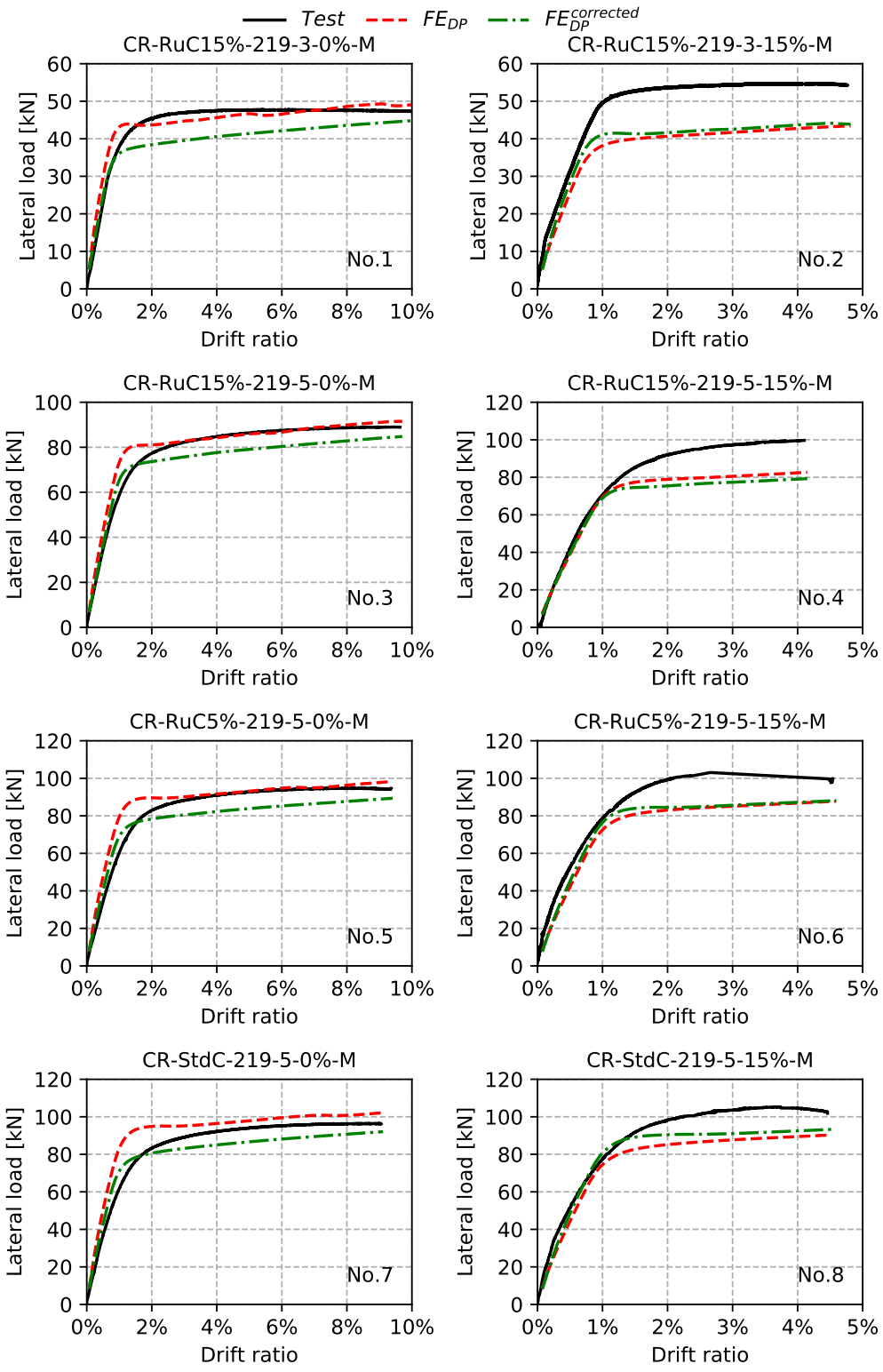

Figure 4: Lateral load versus drift ratio plots comparison between the test results, the two DP models

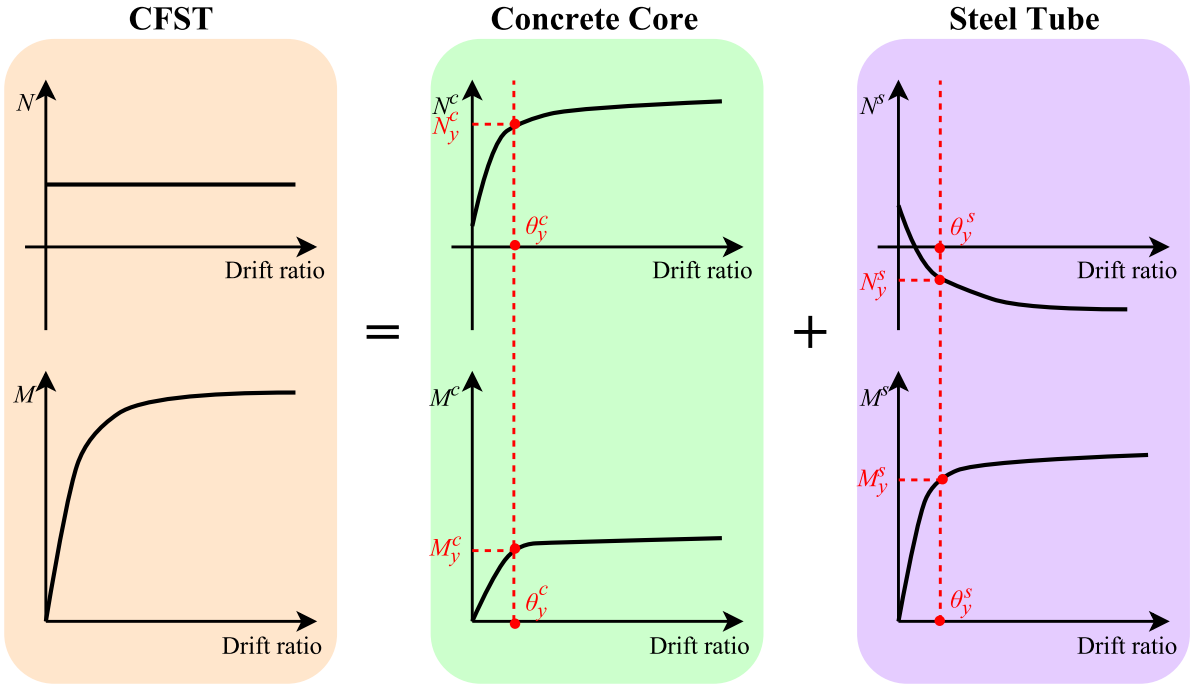

Figure 5: Material strength correction methods schematic diagram

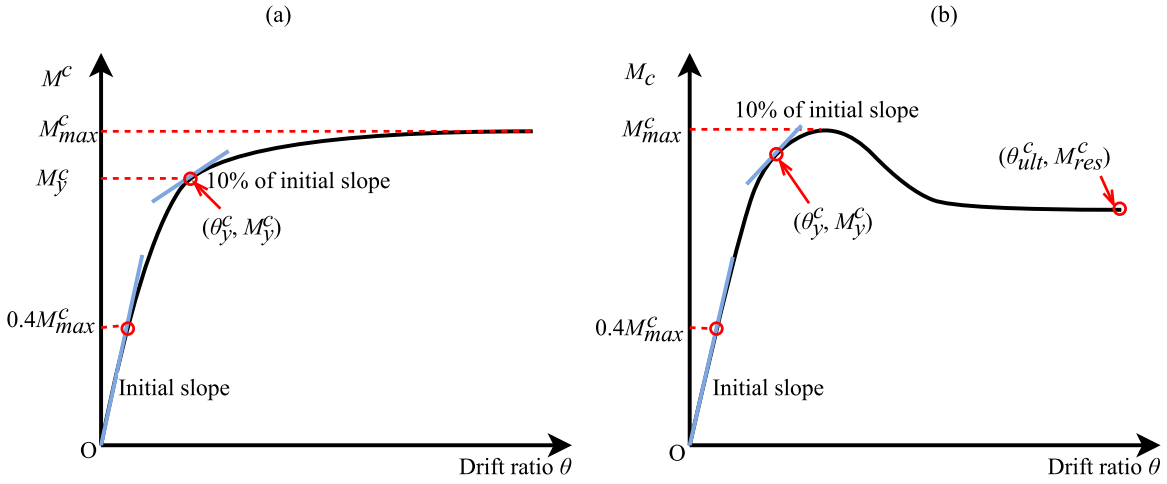

Figure 6: The moment versus drift ratio curves of the concrete core (a) under relatively high confined stress; (b) under relatively low/moderate confined stress

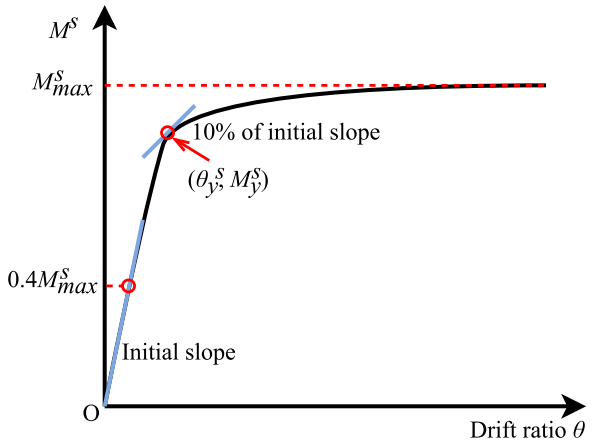

Figure 7: The moment versus drift ratio curves of the steel tube cross-section

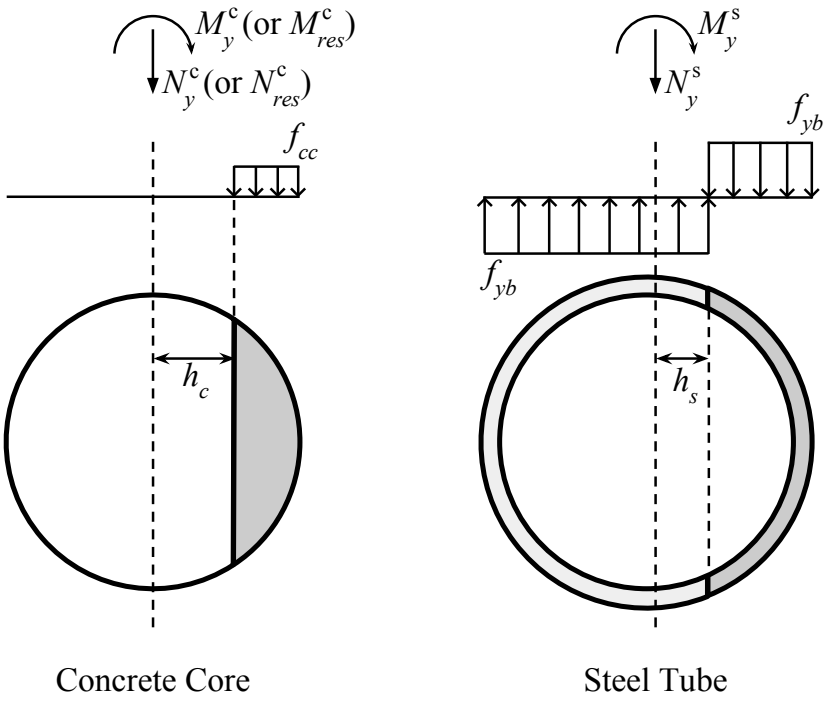

Figure 8: The simplified stress distribution of the concrete and steel sections

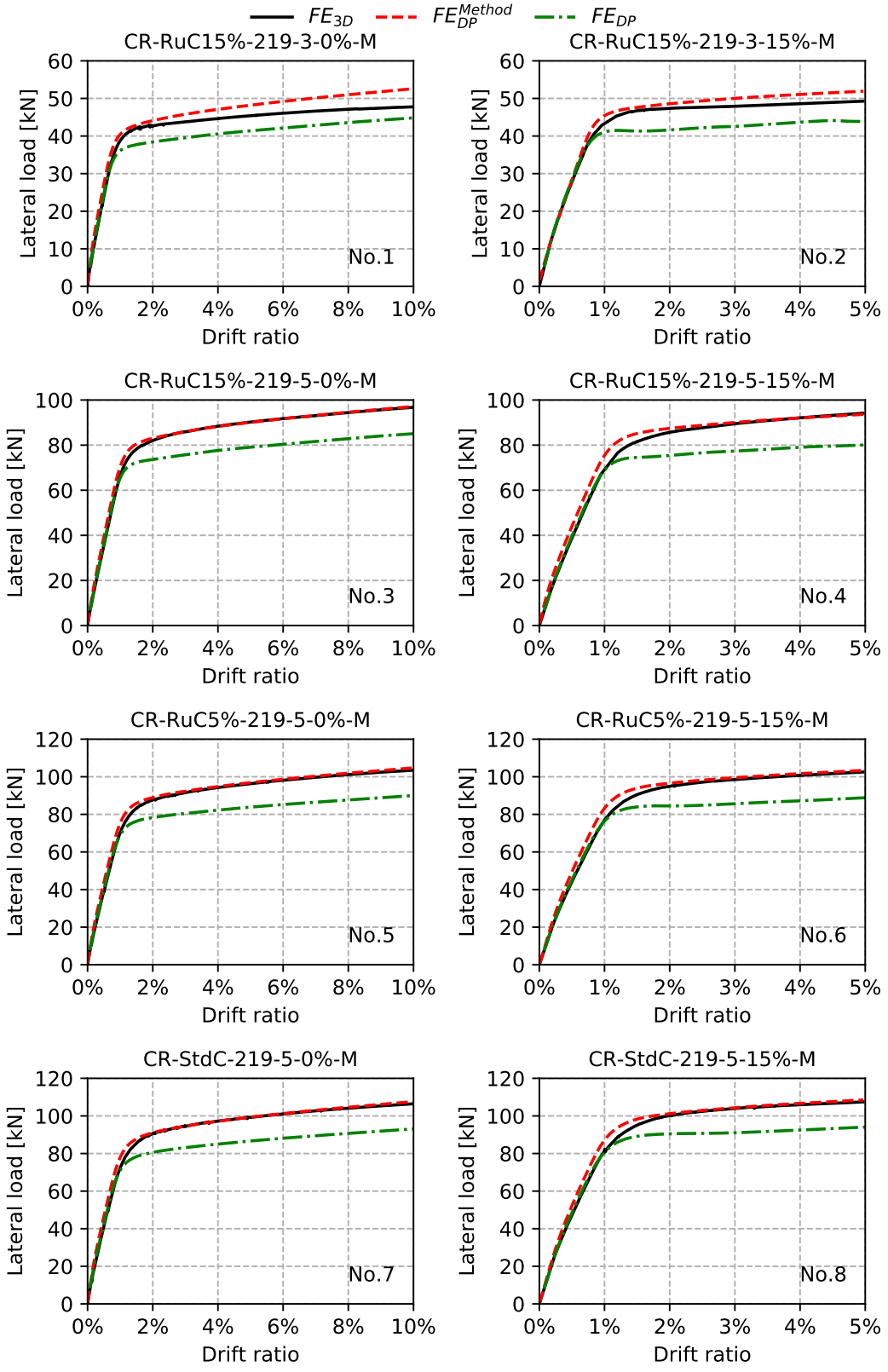

Figure 9: Lateral force-drift ratio curves of the test results and the two DP analyses

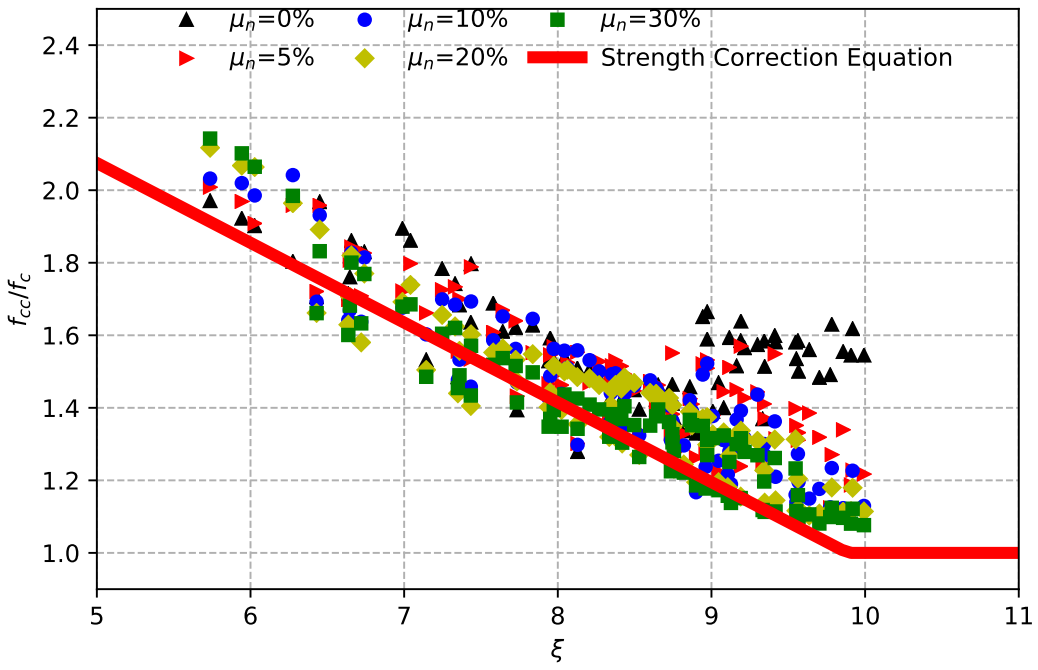

Figure 10: Distribution of confined concrete strengths for each axial load level

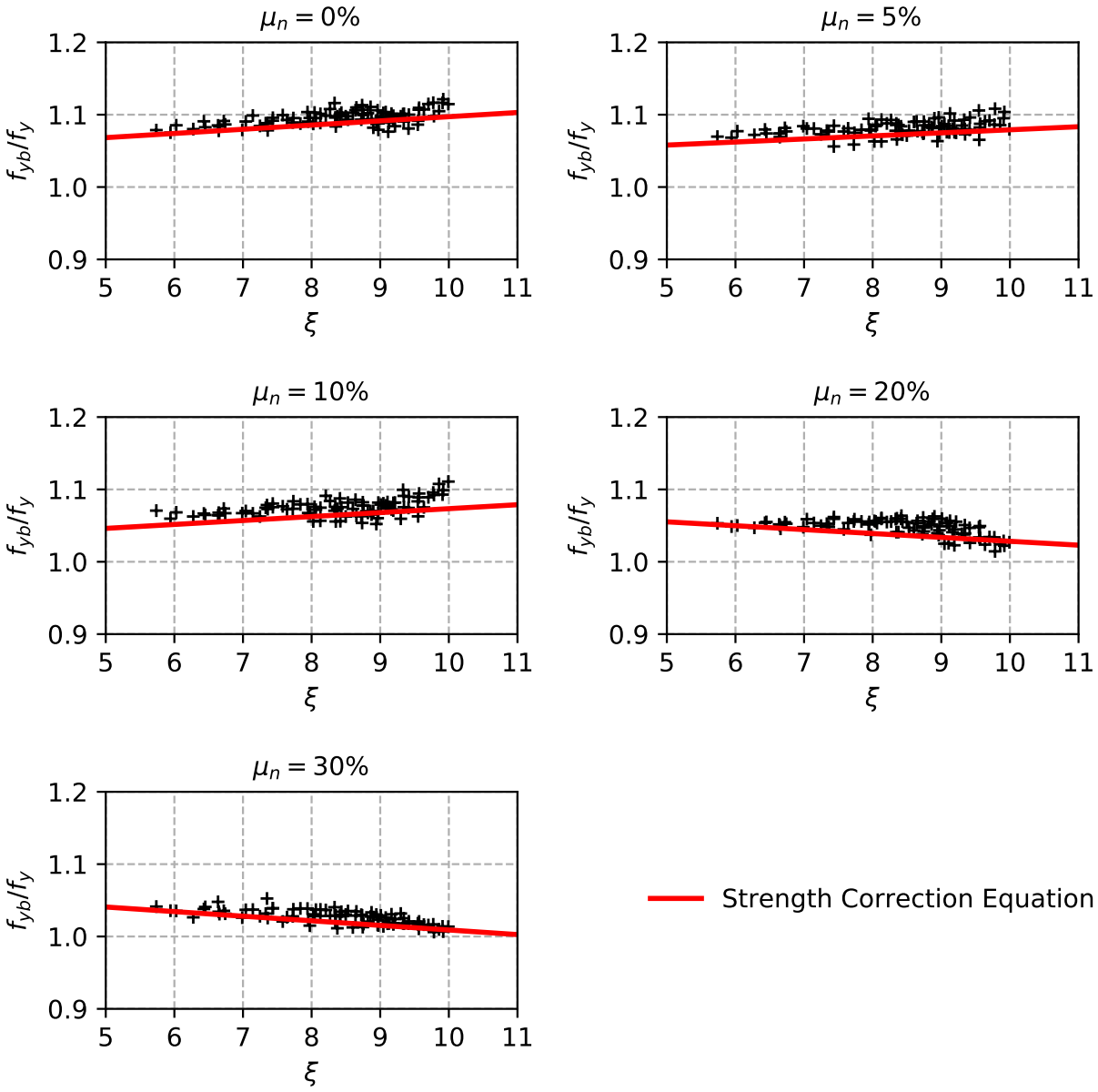

Figure 11: Distribution of steel bi-axial yield strength for each axial load level

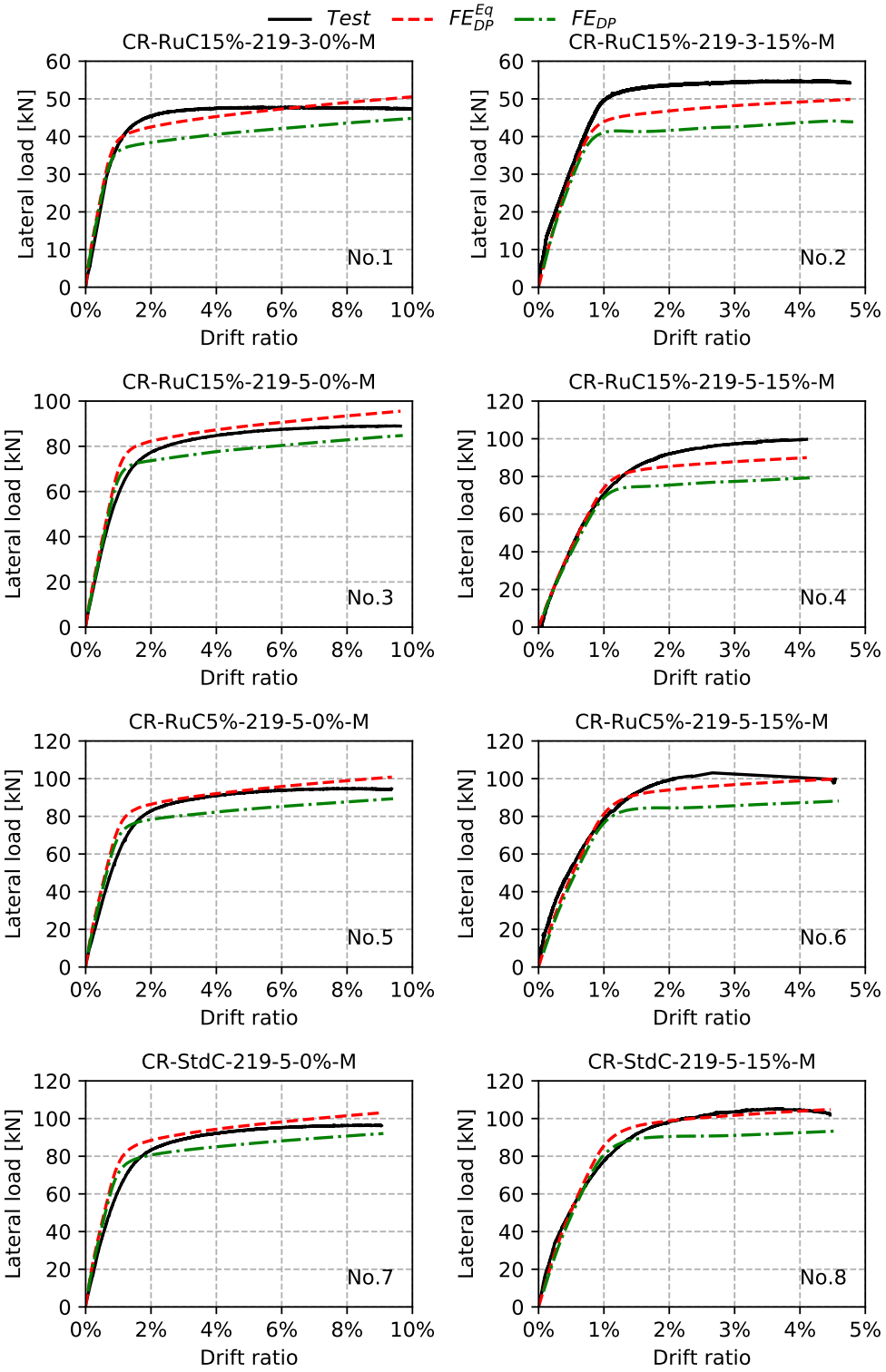

Figure 12: Comparison of the flexural behaviour between the two DP models and the experimental evidence